



Effect of Re-burn Fuel Stream Location on NO Reduction in a Model Pulverized Coal Combustor

Ajay Kumar Sahu and Prakash Ghose*

School of Mechanical Engineering, KIIT Deemed to be University, Patia, P.O. Box 75102, Bhubaneswar, India

Received: 05 January 2021, Revised: 27 April 2021, Accepted: 01 July 2021
© University of Tehran

ABSTRACT

In this work, a computational simulation has been performed to investigate the positional effect of reburn fuel injection on NO-reburn. Reburn fuel methane is injected across the coal injection plane at different axial positions of the combustor. Various major NO source mechanisms are considered for NO formation and NO reburn mechanism is used for NO depletion. Temperature profile, species concentration are also investigated, as both NO formation and depletion rate depends on these parameters. It has been observed that, a high temperature flame exists near coal inlet, when the reburn fuel injection plane is closer to coal inlet. On the other hand, the temperature of the flame near the coal inlet decreases when the reburn fuel injection position is far away from coal inlet region. Moreover, NO sources are observed near coal inlet region, when the reburn fuel is injected closer to coal inlet. On the other hand, only Fuel-NO is observed near coal inlet, when the reburn fuel is injected away from the coal inlet. Maximum NO reduction efficiency is observed at outlet plane when reburn fuel is injected closer to inlet, whereas a relatively lower NO reduction efficiency has been observed at outlet plane when reburn fuel is injected far away from coal inlet region.

KEYWORDS: Oxides of Nitrogen, injection position, coal combustion, computational model.

INTRODUCTION

Coal is relatively a cheaper fuel. Therefore it is preferred in industrial boiler and furnaces as fuel. Formation of oxides of nitrogen (NO_x) during combustion of Pulverized coal and its control is a major challenge in current scenario. It has been observed that, in the flue gas, NO concentration is very high as compared to the other NO_x such as NO₂, N₂O etc.

Also it is more harmful for human body than other NO_x. Majorly three sources of NO formation such as Thermal-NO, Fuel-NO and Prompt-NO which has been observed during coal combustion. Both Thermal-NO and Prompt-NO are formed from atmospheric nitrogen, but they appear in different conditions. On the other hand Fuel-NO is basically generated from the inherent nitrogen presents in coal. In order to meet the pollution control norms, today various methods of NO reduction are used in industries and automotive as well. Low NO_x burner, Over-fire air, NO-reburn, Flue gas recirculation, Flame cooling by water or steam injection etc. are very common methods generally used for NO_x reduction. NO-reburn, using methane as reburn fuel is one of the most effective method, which is preferred in various boilers to minimize NO_x. In this method, methane is generally injected at downstream of the flame. In this process, initially methane bond

* Corresponding Author, Email: pghosefme@kiit.ac.in

breaks in to hydrocarbon radicals such as; CH, CH₂, CH₃ etc. within a temperature range of around 1600 K to 2100K (Bowman, 1991). In the consequent reactions that happen in between NO and hydrocarbon radicals, produces HCN. Further N₂ and other species are formed through subsequent reactions of HCN. Muto et al. (Muto et al., 2015) surmised NO-reburn in PCC process, considering volatile matter is as reburn fuel. Sahu and Ghose (Sahu & Ghose) focused on NO-reburn by using methane as reburn fuel. In both of the work, reburn fuel is injected along the coal particles co-axially within a single cylindrical burner. Muto et al. investigated that, NO-reburn rate is considerably affected by overall equivalence ratio. Sahu and Ghose investigated the effect of coal and reburn fuel (methane) ratio on NO reduction by keeping the total heating value constant as 5 kW. It has been reported that, NO reduction become maximum when the heating contribution by both coal and reburn fuel have 50%. Choi et al. (Choi & Kim, 2009) and Zhang et al. (Zhang, Zhou, Sun, Sun, & Qin, 2015) considered NO-reburn in industrial corner tangentially fired boiler furnaces, where multiple burners are used and volatile matter is used as reburn fuel. Even though NO reburn using volatile matter as reburn fuel has been employed in their work, but it is not discussed much in their study, rather they focused on effect of air staging (OFA) on NO reduction. They concluded that, air staging methodology is an efficient way for NO reduction, where both Thermal-NO and Fuel-NO formation are reduced significantly. Han et al. (Han, Wei, Schnell, Hein, & Flame, 2003) used a premixed methane-ammonia blend as reburn fuel for NO reduction. It has been observed that, when ammonia is used alone as reburn fuel, the NO reduction percentage is around 50%-60%, whereas with a blend of methane it is increased up to 70%-80%. Zarnitz and Pisupati (Zarnitz & Pisupati, 2007) used coal volatile as reburn fuel at downstream of coal burner. In their work, they simulated using volatile gas, methane and diluted volatile gas as reburn fuel separately and it is observed that each reburn fuel gives almost equal benefits regarding NO reduction. Wu et al. (Wu et al., 2004) investigated the effect of syngas as reburn fuel on NO reduction. They compared the effect of reburn fuel injector position on NO reduction. It has been investigated that, co-flow reburn fuel injection methodology is more effective than downstream reburn fuel injection. On the other hand, Su et al. (Su et al., 2007) have performed both experimental and computational work to obtain the optimal position of lateral methane injection point for maximum NO reduction at downstream. Saffari and Weihong (Saffari Pour & Weihong, 2014) developed a very effective and economical method to reduce total NO. They introduced steam along with preheated air to minimize the flame temperature. Eventually Thermal NO decreased up to a great extent as flame temperature decreases.

From the literature review it has been observed that, although NO-reburn has been considered in various works, but detail analysis on reburn has not been done, rather the final NO reduction has been investigated by presenting the NO concentration variation along the combustor /boiler length. In this work, methane is used as reburn fuel, which is injected at three different axial positions across the cylindrical combustor. Here the effect of the methane injection position on NO reduction has been mainly focused. Moreover, in the analysis, the effect of flow pattern, species concentration and temperature on NO formation and NO reduction has been discussed elaborately.

MATERIALS AND METHODS

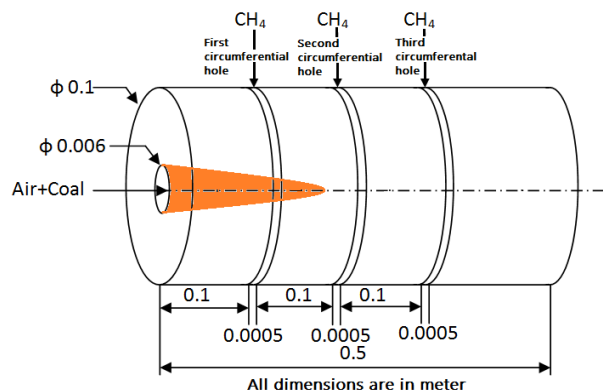
In this simulation, Newlands bituminous coal is used as primary fuel and methane is used as reburn fuel. Different contents of Newlands bituminous coal, those are obtained from Proximate and Ultimate analyses are enlisted below in Table 1. The particle size range used are also given in this table(Hwang et al., 2006).

Table 1. Proximate and Ultimate analysis data for Newlands Bituminous coal.

Proximate analysis [wt%]		Ultimate analysis [wt%]	
Volatile matter ^b	26.90	Carbon ^b	71.90
Fixed carbon ^b	57.90	Hydrogen ^b	4.40
Ash ^b	15.20	Oxygen ^b	6.53
Moisture ^a	2.60	Nitrogen ^b	1.50
		Sulphur ^b	0.44
	Higher calorific value	29.1 MJ/kg	
	Lower calorific value	28.1 MJ/kg	
	Particle maximum diameter	60 µm	
	Particle minimum diameter	5 µm	
	Particle mean diameter	33 µm	

Volatile chemical formula is evaluated from Proximate and Ultimate analysis data as $C_{4.61}H_{4.94}O_{0.46}N_{0.1219}$ (Hashimoto et al., 2012). Molecular weight of the volatile matter and high temperature volatile yielding factor s are taken as 70 and 2.3 respectively (Wen, Jin, Stein, Fan, & Luo, 2015).

A two dimensional axi-symmetric computational domain is prepared for the simulation from the physical geometry as shown in Fig. 1. From the hole having diameter 0.006 m, coal is injected along with carrier air. Three circumferential holes having diameter of 0.0005 m are provided for methane injection at 0.1 m apart. The diameter and length of the combustor is 0.1 m and 0.5 m respectively.

**Fig. 1.** Physical geometry

Pulverized coal combustion is a multiphase problem. Therefore, the entire problem is solved within Eulerian-Lagrangian frame of reference, where numbers of source terms are added in to the Favre averaged gas phase governing equations, in order to incorporate the particle phase effects on gas phase and vice versa. The governing equations used for simulation are given as follows;

Conservation of mass

$$\frac{\partial}{\partial x_i}(\bar{\rho} \tilde{u}_i) = S_m \quad (1)$$

Conservation of momentum

$$\frac{\partial}{\partial x_i}(\bar{\rho} \tilde{u}_i \tilde{u}_j) = -\frac{\partial \bar{p}}{\partial x_i} + \frac{\partial}{\partial x_i}(\bar{\tau}_{ij} - \bar{\rho} u_i'' u_j'') + S_s \quad (2)$$

Conservation of general scalar variable

$$\frac{\partial}{\partial x_i} (\bar{\rho} \tilde{u}_j \tilde{\varphi}) = \frac{\partial}{\partial x_i} \left(\Gamma_{\phi,eff} \frac{\partial \tilde{\varphi}}{\partial x_i} \right) + S_{\phi,s} \quad (3)$$

In equation 3, φ is scalar variable, which is enthalpy in energy equation and species concentration in species transport equations. In energy conservation equation, $\Gamma_{\phi,eff} = (\Gamma_{\phi,lam} + \Gamma_{\phi,tur}) = \left(\frac{\mu}{\sigma} + \frac{\mu_t}{\sigma_t} \right)$, whereas in species conservation equation $\Gamma_{\phi,eff} = (\Gamma_{\phi,lam} + \Gamma_{\phi,tur}) = \left(\frac{\mu}{Sc} + \frac{\mu_t}{Sc_t} \right)$. For evaluation of Reynolds stresses of momentum equations, Boussinesq hypothesis for eddy viscosity modelling is used as;

$$-\bar{\rho} u_i'' u_j'' = \mu_t \left(\frac{\partial \tilde{u}_i}{\partial x_j} + \frac{\partial \tilde{u}_j}{\partial x_i} \right) - \frac{2}{3} \bar{\rho} \tilde{k} \delta_{ij} \quad (4)$$

where $\mu_t = \rho C_\mu \frac{k^2}{\varepsilon}$. In order to calculate eddy viscosity (μ_t) and Reynold stresses, transport equation for k , ε are solved with the help of Standard k - ε model (Launder & Spalding, 1983). The inter-phase source terms for different governing equations are discussed in following sections.

Forty numbers of coal particle classes having minimum, maximum and mean diameter as given in Table 1., are injected along with the primary air. The spread parameter of 4.02 is used to calculate particle diameter distribution by following Rosin-Ramellar distribution scheme (Ghose, Patra, Datta, & Mukhopadhyay, 2016). The particle dispersion due to gas phase turbulence effect are simulated by employing Discrete random walk model (Gorenflo, Mainardi, Moretti, Pagnini, & Paradisi, 2002). A force balance equation is solved to evaluate the drag force exerted on droplet by gas phase and vice versa is expressed as;

$$m_p(j) \frac{du_{p_i}}{dt} = \frac{\pi}{8} \rho_p [d(j)]^2 |u_i - u_{p_i}(j)| [u_i - u_{p_i}(j)] C_{drag} \quad (5)$$

In the above equation the drag coefficient is calculated by following the spherical drag law (Morsi & Alexander, 1972), expressed as; , where a_1, a_2, a_3 are model constants and $Re \left(= \frac{\rho |u_i - u_{p_i}(j)| d_j}{\mu} \right)$ is the Reynolds number considering the flow over spherical particles.

In order to incorporate the mass exchange in between particle and gas phase, a mass balance equation is solved, that is expressed as;

$$\frac{dm_p(j)}{dt} = \frac{dm_{vol}(j)}{dt} + \frac{dm_{char}(j)}{dt} \quad (6)$$

where $\frac{dm_{vol}(j)}{dt}$ and $\frac{dm_{char}(j)}{dt}$ are volatile evolution rate and particle mass depletion rate due to char combustion. Mathematical expressions of these rates are elaborated in the following sections.

Heat energy balance equation is also solved to include the effect of heat energy exchange in between two phases occurs by convection, radiation and coal burnout. Mathematically the energy balance equation is expressed as;

$$m_p(j) c_{p_s} \frac{dT_p}{dt} = h_c A_p (T - T_p) + \varepsilon 1_p A_p \sigma (\theta_R^4 - T_p^4) - f_h \left(\frac{dm_{vol}(j)}{dt} \Delta H_v + \frac{dm_{char}(j)}{dt} \Delta H_c \right) \quad (7)$$

The inter-facial convective heat transfer coefficient (h_c) is evaluated with the help of Nusselt number correlation suggested by Ranz and Marshal (Ranz & MarShal, 1952). A considerable amount of heat is radiated from the flame due to large temperature difference in between flame and ambient. In addition to that, presence of soot in flame enhances the heat loss from the flame. Therefore in bulk gas absorption coefficient absorptivity of soot is also included. In this work, Weighted sum gray gas model (WSGGM) (Yu, Baek, & Kang, 2001) is used to determine the bulk gas absorption coefficient. In order to evaluate radiation intensity, Discrete Ordinate (DO) (Fiveland, 1988) radiation modelling method is employed for solving the radiative transport equation (RTE), where bulk gas is considered as participating media. The radiative temperature θ_R is calculated as; $\theta_R = \left(\frac{\int_{\Omega=4\pi} Id\Omega}{4\sigma} \right)^{1/4}$. However, scattering and transmission effect is neglected in gas phase, while both absorption and scattering are considered for particle phase. The last term in the above equation is the heat transfer from particle surface due to volatile and char combustion. Khan and Greeves soot model (Backreedy et al., 2006) is used to include the effect of soot on field temperature.

The mass depletion rate of jth particle due to volatile evolution or volatile evolution rate is calculated with the help of single rate kinetic model (Ansys Fluent Theory Guide) is expressed as;

$$\frac{dm_{vol}(j)}{dt} = k \left[m_p - (1 - P_{vol_0}) m_{p0} \right] \quad (8)$$

Here, the reaction rate coefficient; $k = Ae^{-(E/RT)}$, where A is the frequency factor ($A = 4.747 \times 10^5$) and E is the activation energy ($E = 7.4 \times 10^6$). For char combustion, Intrinsic char reaction model (Backreedy et al., 2005) is used. The rate of depletion of jth char particle mass or the char reaction rate is expressed as;

$$\frac{dm_{char}(j)}{dt} = -A_p \frac{\rho R T Y_{ox}}{MW_{O_2}} \frac{D_0 \mathfrak{R}}{D_0 + \mathfrak{R}} \quad (9)$$

In Intrinsic char combustion model, the effect of oxygen diffusion towards the core of coal particle is accounted, hence, the effect of coal porosity and porous hole twist are regarded as well. In the above equation, D_0 and \mathfrak{R} denoted the oxidant diffusion rate coefficient and chemical reaction rate considering physical nature of the coal respectively and A_p is the particle surface area. Here the chemical reaction rate is evaluated by using Arrhenius rate coefficient.

Four combustion reactions (R-1 to R-4) are used in this simulation. Out of them, R-1, R-2 and R-3 are first step reactions where CO is the major product. In reaction R-4, CO reacts with O_2 to form final product CO_2 .



Eddy dissipation model (Magnussen & Hjertager, 1977) is used for determination of gas phase reaction rate is expressed as;

$$\tilde{\omega}_{EDM} = \underbrace{B\bar{\rho} \frac{\varepsilon}{k} \times \tilde{Y}_f}_{RR1} (or) \underbrace{B\bar{\rho} \frac{\varepsilon}{k} \times \frac{\tilde{Y}_{O_2}}{\gamma}}_{RR2} (or) \underbrace{B\bar{\rho} \frac{\varepsilon}{k} \times \frac{B_1 \sum \tilde{Y}_p}{1+\gamma}}_{RR3} \quad (10)$$

In the above equation, out of three reaction rate (*RR1 to RR3*), the smallest rate of reaction is used as reaction rate in gas phase combustion. Here, B and B_1 are the model constants and their value are taken as 4 and 0.5 respectively. \tilde{Y}_f , \tilde{Y}_{O_2} , \tilde{Y}_p and γ are mass fraction of fuel, oxygen, products and local equivalence ratio respectively.

In PCC, there are three major sources of NO formation. Out of them, Thermal-NO and Prompt-NO are formed with the presence of atmospheric nitrogen, but the conditions for NO formation reactions are different for both of them. While Fuel-NO originates from the inherent nitrogen presents in coal particle.

Thermal-NO formation rate is evaluated by following the well known extended Zeldovich mechanism (Choi & Kim, 2009).



In extended Zeldovich mechanism, the formation and depletion rate of N atom is very high. Therefore, Quasi-steady assumption is applied to nitrogen atom and the rate of Thermal-NO is derived as;

$$\frac{d[X_{NO}]}{dt} = 2k_{f,1}[X_O][X_{N_2}] \frac{\left(1 - \frac{k_{r,1}k_{r,2}[X_{NO}]^2}{k_{f,1}[X_{N_2}]k_{f,2}[X_{O_2}]}\right)}{\left(1 + \frac{k_{r,1}[X_{NO}]}{k_{f,2}[X_{O_2}] + k_{f,3}[X_{OH}]}\right)} \text{ mol/m}^3\text{-s} \quad (11)$$

where molar concentration of O and OH are evaluated as; $[X_O] = 3.97 \times 10^5 T^{-1/2} \exp^{-31090/T} [X_{O_2}]^{1/2}$ and $[X_{OH}] = 2.129 \times 10^2 T^{-0.57} \exp^{-4595/T} [X_O]^{1/2} [X_{H_2O}]^{1/2}$ respectively (Ansys Fluent Theory Guide).

Within the fuel rich zone under moderate temperature, hydrocarbon radicals appear. That reacts with atmospheric nitrogen and produces HCN. Consequent reactions of HCN with other species generate Prompt-NO. The Prompt-NO formation rate proposed by De Soete (De & DE SOETE, 1974) is expressed as;

Table 2. Input parameters to NO models

Fuel	Fuel-NO			Prompt-NO			BET surface area (m ² /kg)	Fuel carbon number	Equivalence ratio
	Total nitrogen content	Nitrogen mass fraction	Nitrogen convertible to NO	%age of nitrogen allowed to convert HCN, NH ₃ and direct NO					
				HCN	NH ₃	NO			
Volatile	30%	0.0168	90%	80%	20%	0	25000	4.61	7.51
Char	70%	0.01827	90%	0	0	100%	-	-	-
Methane	-	-	-	-	-	-	-	1	1.217

$$\frac{d[X_{NO}]}{dt} = f k_{pr} [X_{O_2}]^a [X_{N_2}] [X_{fuel}] \exp^{-E_a/RT} \quad (12)$$

In the above equation f is a correction factor that depends on carbon atom number of fuel and the equivalence ratio within the reaction zone. k_{pr} is the NO production rate coefficient. a is reaction order for oxygen depends up on the oxygen molar fraction within the reaction zone.

During the reaction, inherent nitrogen present in fuel produces intermediate species such as; HCN and NH₃. The consequent reactions of HCN and NH₃ with O₂, forms NO. However a fraction of NO again depletes by reacting with HCN/NH₃ to N₂. A significant amount of fuel nitrogen also directly forms NO. The source term for HCN, NH₃ and NO are expressed in ref. (Choi & Kim, 2009). The HCN and NH₃ depletion rate are expressed as;

$$\frac{d[X_{HCN}]}{dt} \Big|_{O_2 \rightarrow NO} = k_1 [X_{HCN}] [X_{O_2}]^a e^{-E_1/RT} \frac{MW_{NO} P}{RT} \quad (13a)$$

$$\frac{d[X_{HCN}]}{dt} \Big|_{NO \rightarrow N_2} = -k_2 [X_{HCN}] [X_{NO}] e^{-E_2/RT} \frac{MW_{NO} P}{RT} \quad (13b)$$

$$\frac{d[X_{NH_3}]}{dt} \Big|_{O_2 \rightarrow NO} = k_3 [X_{NH_3}] [X_{O_2}]^a e^{-E_3/RT} \frac{MW_{NO} P}{RT} \quad (13c)$$

$$\frac{d[X_{NH_3}]}{dt} \Big|_{NO \rightarrow N_2} = -k_4 [X_{NH_3}] [X_{NO}] e^{-E_4/RT} \frac{MW_{NO} P}{RT} \quad (13d)$$

Nitrogen content in coal and their conversion fractions which are used in this work is given in table 2.

In NO re-burning process, NO converts majorly to HCN by reacting with hydrocarbon radicals (CH, CH₂, CH₃...). These radicals are formed from reburn hydrocarbon fuel dissociation. Therefore a strong NO-reburn zone can be observed at reburn fuel rich zone, along with the presence of NO. The reaction mechanisms of NO with hydrocarbon radicals are globally expressed as;



In order to evaluate the NO depletion rate, partial equilibrium approximation approach is used (Su et al., 2006), where NO depletion rate and HCN formation rates considering CH₄ is reburn fuel are expressed as;

$$\frac{d[X_{HCN}]}{dt} = 4 \times 10^{-4} \left\{ (k_a \chi_1 + k_b \chi_1^2) [X_{CH_4}] [X_{NO}] \right\} \quad (15)$$

$$\frac{d[X_{NO}]}{dt} = -4 \times 10^{-4} \left\{ (k_a \chi_1 + k_b \chi_1^2) [X_{CH_4}] [X_{NO}] + (k_c \chi_1^3 \chi_2) [X_{CH_4}] [X_{NO}] \right\} \quad (16)$$

where $\chi_1 = \frac{X_H}{X_{H_2}}$; Its value is taken as one by assuming that hydrogen radical H is observed as same order with H₂ near post flame region in non premixed flame. $\chi_2 = \frac{X_{OH}}{X_{H_2O}}$, where mole

fraction of OH radical is obtained from the reaction; $OH + H_2 \xrightleftharpoons[k_{r1}]{k_{f1}} H_2O + H$

The rate constants $k_a, k_b, k_c, k_{f1}, k_{r1}$ for different re-burn fuel are used from the work Leung et al. (Leung & Lindstedt, 1995).

RESULTS AND DISCUSSION

An axi-symmetric model is prepared by following the experimental setup of Hwang et al. (Hwang et al., 2006) where Newlands Bituminous coal is used along with co-flow methane. Therefore, for validation Newlands Bituminous coal is injected along with co-flow methane. However, various computational models those are discussed in previous sections are used for this simulation.

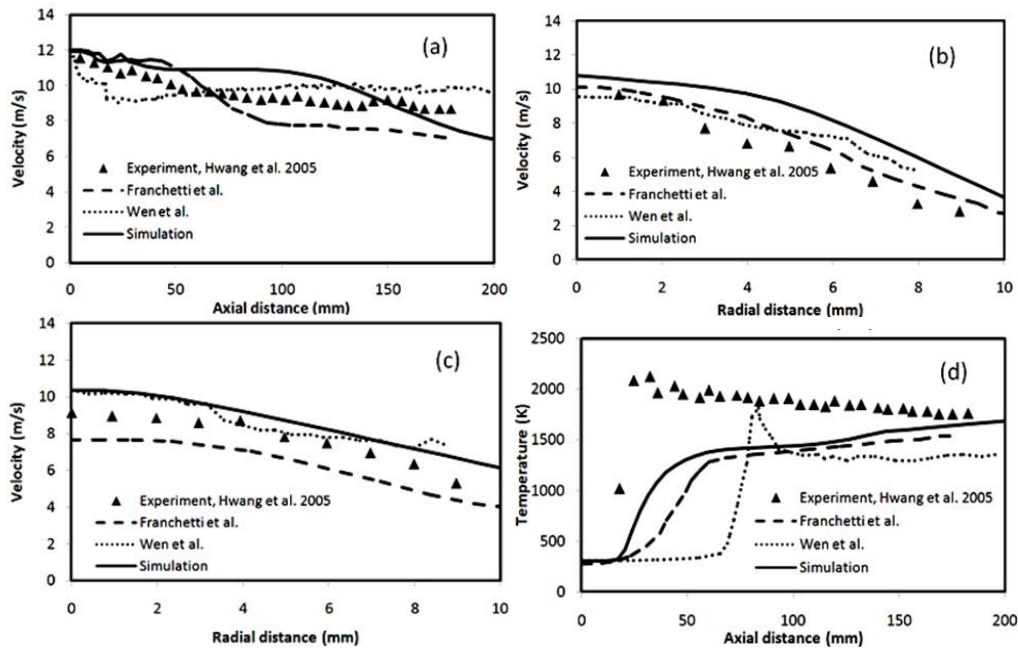


Fig. 2. Axial velocity distribution (a) along the combustor axis (b) along radial direction at axial position 60 mm from inlet (c) along radial direction at axial distance 120 mm from inlet. (d) Temperature comparison along the axis

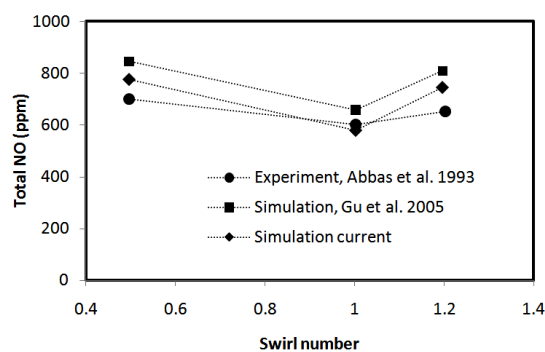


Fig. 3. Mass weighted average of net NO at burner outlet for different secondary air swirl number

From fig. 2a-2d it is observed that, the current simulation little bit over predict the axial velocity and the radial distribution of axial velocity, whereas temperature prediction along the axis is better than Wen et al. and Franchetti et al. (Franchetti, Marincola, Navarro-Martinez, & Kempf, 2013; Wen et al., 2015). However a separate simulation has also been accomplished by following the experimentation of Abbas et al. (Abbas, Costen, Hassan, & Lockwood, 1993) for the validation of NO. Moreover the result is compared with the simulation of Gu et

al. (Gu, Zhang, Fan, Wang, & Tian, 2005). From fig. 3, it can be observed that, the NO is fairly predicted by the computational models used in current computational simulation.

In this work, pulverized coal particles are injected along with primary air through a central hole. In order to inject reburn fuel (methane) laterally, three circumferential holes are made at the interval of 0.1m from inlet plane as shown in Fig. 1. In case A, the reburn fuel is injected through first circumferential hole and the remaining two traversed hole are closed. In case B first and third traversed holes are closed and methane is injected through second traversed hole only. In case C, third hole is opened and first and second traversed holes are closed. The operating conditions are shown in Table 3.

Table 3. Operating conditions

Description	Case A	Case B	Case C
First circumferential hole	<i>opened</i>	closed	closed
Second circumferential hole	closed	<i>opened</i>	closed
Third circumferential hole	closed	closed	<i>opened</i>
Methane mass flow rate (kg/s) (Reburn Fuel)		6.192×10^{-4}	
Air mass flow rate (kg/s)		0.0003	
Coal mass flow rate (kg/s)		1×10^{-5}	
Overall equivalence (ϕ) ratio considering coal only as fuel		0.58	

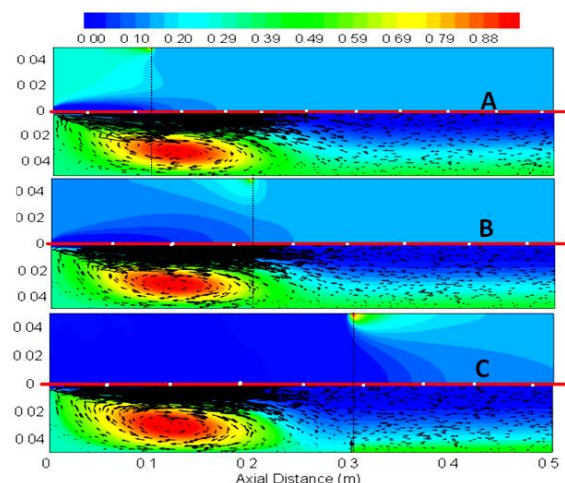


Fig. 4. Methane concentration (top half), velocity vector and stream function (bottom half) for case A, B and C

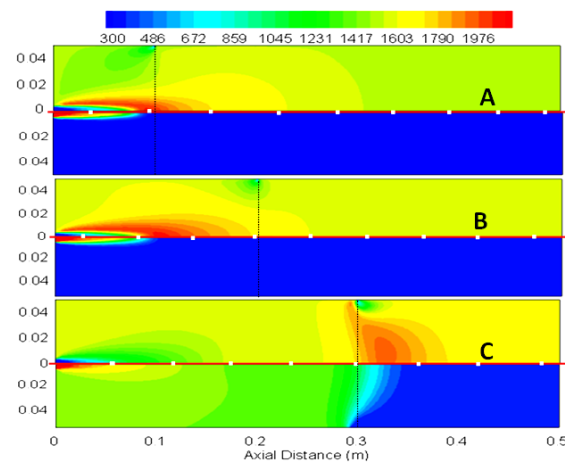


Fig. 5. Temperature in Kelvin (top half), Oxygen concentration (bottom half) for case A, B and C

Fig. 4 depicts the methane diffusion for case A, B and C. In this Fig., methane concentration is shown in top half and stream function-velocity vector is shown in bottom half. It is obvious that due to sudden expansion, a corner recirculation zone (CRZ) is formed near inlet region and the reattachment length is around 0.25 m from inlet.

For case A and B it has been observed that, radially injected methane is falling within the area of the recirculation zone. In these cases, maximum fraction of the injected methane is pulled and diffused into the recirculation zone due to adverse pressure gradient. The overall equivalence ratio ϕ is 0.58 (lean mixture) as shown in table 3. However, with the addition of diffused methane, a better mixture (closed to stoichiometric) has been formed along with char and volatile near inlet region. From Fig 5 A and B (Top half temperature contour and bottom half oxygen concentration), it is evident that, due to ideal air-fuel mixture, maximum fraction of oxygen has been utilized for combustion. Hence a high temperature flame is established near inlet region. On the other hand in case C, the radially injected methane travelled towards downstream, rather moving back towards inlet region. It is because the injection hole is far away from recirculation zone. Therefore like case A and B, a proper mixture cannot be prepared near inlet in case C, hence the region remains with lean mixture. As a result, in this region the flame become over cooled by the excess air, as a consequence, the flame temperature decreased as shown in fig 5 C. From this figure it is obvious that, the excess oxygen diffused and prepares a combustible mixture near methane injection plane (0.3 m from inlet). In this region, the excess oxygen reacts with methane and produces a higher temperature zone as shown in Fig. 5 C.

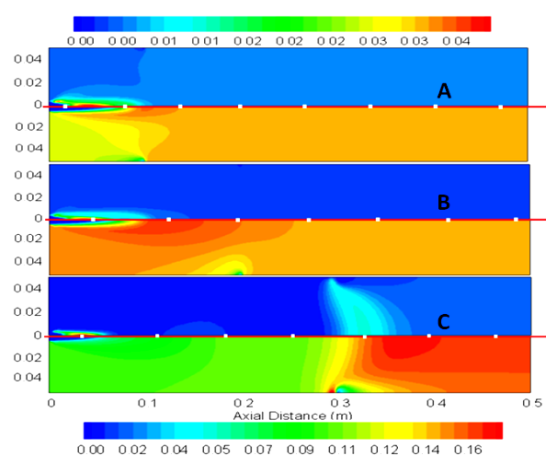


Fig. 6. CO concentration (top half), CO₂ concentration (bottom half) for case A, B and C

Reaction R-1 to R-3 are the reactions equations for volatile, methane and char with air, where the intermediate species CO forms. For case A and B, CO concentration is high near inlet region as shown in Fig. 6 A and B. Because reactions R-1 to R-3 takes place together in this region due to presence of volatile, char, methane and oxygen at a proper ratio. However, relatively higher concentration of CO is observed in case A, because a better methane concentration is available within flame region, as the methane injection hole is much closer to flame than case B. But in Fig. 6 C, two CO concentration zones have been observed. The CO zone near inlet is due to reactions R-1 and R-3, whereas CO concentration at downstream is due to reaction R-2 (methane-air reaction) only. Because in case C, methane could not be pulled back towards inlet, as the injected methane stream does not fall into the recirculation zone.

Reaction R-4 is the source of CO₂, where the intermediate species CO reacts with oxygen. The bottom half of Fig. 6 A-C depicts CO₂ concentration. In case A, little higher concentration of methane dilutes the mixture, therefore a relatively lower CO₂ concentration is observed closer to inlet in case A as compared to case B. On the other hand in case C, less

amount of CO₂ formed at inlet flame region, due to presence of smaller concentration of CO and lower reaction temperature. But at downstream (near methane injection cross section), intermediate CO reacts with extra oxygen. However, it is already discussed that due to absence of methane at inlet region, the mixture became lean and the excess oxygen or extra oxygen flows and diffuse along downstream, which reacts with intermediate CO to form CO₂.

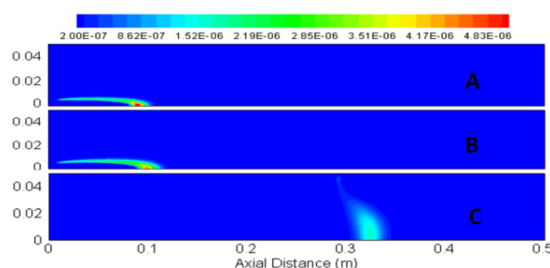


Fig. 7. Rate of Thermal-NO ($\text{kmol/m}^3\text{-s}$) for case A, B and C

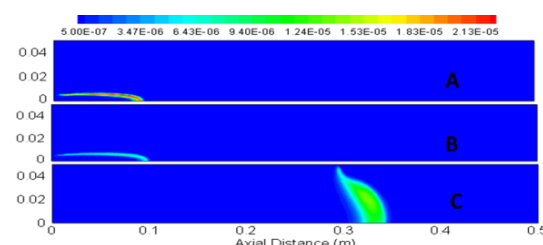


Fig. 8. Rate of Prompt-NO ($\text{kmol/m}^3\text{-s}$) for case A, B and C

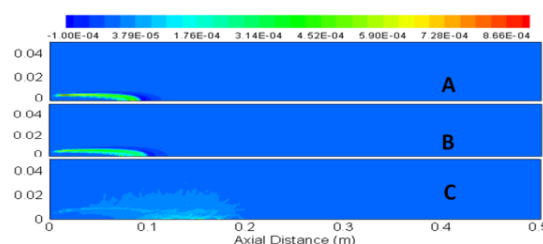


Fig. 9. Rate of Fuel-NO ($\text{kmol/m}^3\text{-s}$) for case A, B and C

Fig. 7 to 9 depicts the rate of formation of NO in $\text{kmol/m}^3\text{-s}$, by three different mechanism such as; Thermal-NO, Prompt-NO and Fuel-NO respectively for the cases A, B and C. It is well known that, Thermal-NO depends upon flame temperature, availability of atmospheric O₂ and N₂. Similarly, Prompt-NO reaction rate is also related to atmospheric N₂, where N₂ reacts with hydrocarbon radicals to form intermediate species. The consequent reactions happen in between intermediate species with O₂ and oxygen radicals produces Prompt-NO. Therefore Prompt-NO formation rate become high within the fuel rich zone at moderate temperature. But if local equivalence ratio becomes too high, Prompt-NO decreases due to deficit in O₂. On the other hand, Fuel-NO is the conversion of inherent nitrogen presents in coal to NO directly and/or through intermediate reaction of HCN and NH₃.

Since, both flame temperature and air (N₂ and O₂) concentration is nearly same in the case A and case B, the value of Thermal-NO formation rate is also closer to each other. On the other hand, in case C, no Thermal-NO formation is observed at inlet flame region. Because N₂ dissociation and NO formation is possible only with higher temperature (around greater than 1800K), but here the maximum flame temperature is around in between 1200 K to 1400 K. But in this case C, a moderate but wider Thermal-NO formation region is detected at downstream (near methane injection cross section). In this region a favourable temperature and N₂ field are mainly responsible for Thermal-NO formation.

It is already discussed that, with moderate temperature, hydrocarbon radical formation rate become high within the fuel rich zone. From Fig. 5, one can see that, case B has the highest flame temperature as compared to case A and C. Therefore in case B, very high flame temperatures lessen the hydrocarbon radicals formation at inlet reaction zone. As a result in this case, least Prompt-NO rate is observed in this region due to scarcity of hydrocarbon radicals. In case C, the reactions for Prompt-NO could not even start in this region due to very low flame temperature (1200 K to 1400 K). But at downstream (near methane injection cross section), in case C, moderate Prompt-NO formation is observed. In this region, a favourable temperature field and N_2 concentration is available to form Prompt-NO.

Even though the process of Fuel-NO formation is much complicated as compared to Thermal and Prompt-NO, but it can be predicted easily. From temperature contour as shown in Fig. 5, it is clear that, volatile evolution, volatile combustion and char burnout takes place near inlet. During these processes, the evolved inherent coal nitrogen partially reacts with O radical to form Fuel-NO. Moreover, the consequent reactions of newly formed HCN and NH_3 precursor (formed by inherent nitrogen) generate Fuel-NO. However the entire reaction takes place near inlet region. Therefore a higher Fuel-NO formation rate is observed near inlet region in all the cases. As flame temperature is high in case A and B, a higher Fuel-NO evolution can be seen here. Whereas in case C, a lower flame temperature is the sole reason for low Fuel-NO evolution.

Upper half of Fig. 11 shows the NO concentration without considering NO-reburn reactions. However NO concentration is the sum of NO formed through Thermal-NO, Prompt-NO and Fuel-NO. For the cases A and B, NO concentration is observed at inlet flame region, because the aforesaid three different sources for NO are observed at the same location. On the other hand, in case C, due to existence of a stronger Prompt-NO sources across methane injection plane, NO concentration is too high in this region. Moreover NO is well diffused throughout the domain due to higher NO concentration in this case.

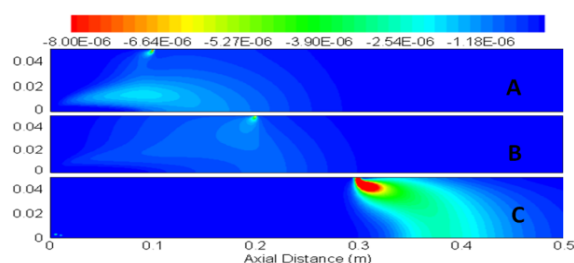


Fig. 10. NO-reburn rate ($kmol/m^3 \cdot s$) for case A, B and C

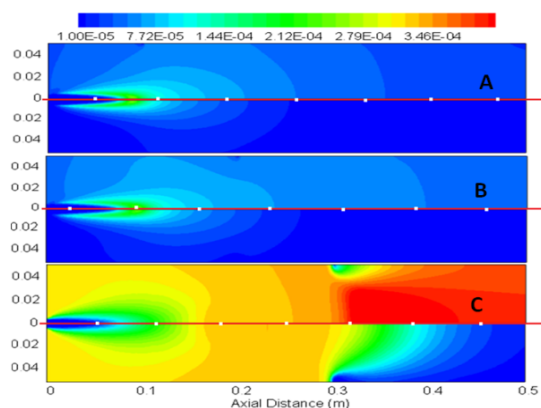


Fig. 11. NO concentration without reburn (top half), NO concentration with reburn (bottom half) for case A, B and C

Fig. 10 shows the reburn rate for all three cases. In NO re-burning process, NO converts majorly to HCN by reacting with hydrocarbon radicals (CH, CH₂, CH₃...). These radicals are formed through the breaking of the bond of hydrocarbon reburn fuel. However in this work methane (CH₄) is the reburn fuel. NO-reburn reaction occurs within a temperature range around 1600K to 2100K (Bowman, 1991). From the rate coefficients of NO-reburn reaction mechanism Proposed by Bowman (Bowman, 1991), it is noticed that, within the NO-reburn reaction zone, as temperature increases, NO depletion rate decreases and vice versa. More importantly, a higher NO-reburn rate can be expected at the higher NO concentration region.

Near methane inlet region, a better reburn rate has been observed due to higher hydrocarbon radical concentration and favourable temperature for all the cases. In case B, due to highest flame temperature, the reburn reaction rate is the lowest among all the cases within the flame region. In case C, across methane injection plane area, NO-reburn rate is too high, because higher concentration of NO and availability of methane, enhances the NO-reburn rate in this location. However within the region, where hydrocarbon radical concentration is very poor and temperature is below 1600, NO-reburn reaction is not at all possible there, hence no NO rate contour is observed in these locations.

Fig. 11 gives a comparative picture of NO concentration without considering reburn mechanism (top half of the figure) and with considering reburn mechanism (bottom half of the figure). Fig. 12 a and 12 b depicts the mass weighted average of NO concentration across 10 different planes along the axial line without considering reburn and with considering reburn mechanism respectively for case A, B and C. Fig. 12 c, illustrates the NO reduction efficiency along the axial line. The NO reduction efficiency is calculated as;

$$\text{NO reduction efficiency} = \frac{\text{NO}_{\text{without reburn}} - \text{NO}_{\text{with reburn}}}{\text{NO}_{\text{without reburn}}} \times 100 \quad (17)$$

Fig. 12 a, can be described through the observation of upper half of Fig. 11. Since, the sources of Thermal-NO, Prompt-NO and Fuel-NO exist near inlet flame region, In case A and B a higher NO ppm is observed near inlet. Due to diffusion and convection NO also exist along downstream but slowly decreasing. On the other hand in case C, maximum NO in ppm is observed just beyond methane injection plane along downstream. Because in this case, Prompt-NO and Thermal-NO concentration is very high in this region. Moreover in this case both Prompt-NO and Thermal-NO is higher as compared to case A and B. In case C, due to presence of Fuel-NO and more predominantly due to diffusion of Thermal-NO and Prompt-NO, one can see a decreasing NO line towards inlet. In this case, exactly at $x=0.3$, NO concentration is suddenly dropped, because here methane occupies a fraction of volume.

Fig. 12 b, can be described through the observation of lower half of Fig. 11. With the consideration of NO-reburn, NO reduction can be observed along the axis, in cases A and B, whereas NO reduction in case C is observed from 0.25 m up to the exit of the burner. It is obvious that, as in case A and B methane injection is closer to flame NO reduction starts at closer to inlet. On the other hand, as methane injection is done in case C at 0.3 m downstream, NO reduction starts near this region.

NO concentration decreases with considering NO-reburn along axial direction in cases A and B. Therefore in these cases, NO reduction efficiency increases along the axial direction as shown in fig 12 c. NO concentration become zero beyond 0.25 m from inlet with the consideration of NO-reburn. As a result, 100% NO reduction is obtained beyond these positions in case A and B. On the other hand in case C, NO-reburn does not occur up to 0.25 m from inlet due to absence of reburn fuel. As a result 0% NO reduction occurs within this region. But, after 0.25 m from inlet, NO reduction percentage increases, because NO-reburn

rate is much higher in this region due to presence of reburn fuel. But still at exit, only 98% NO reduction was possible in this case.

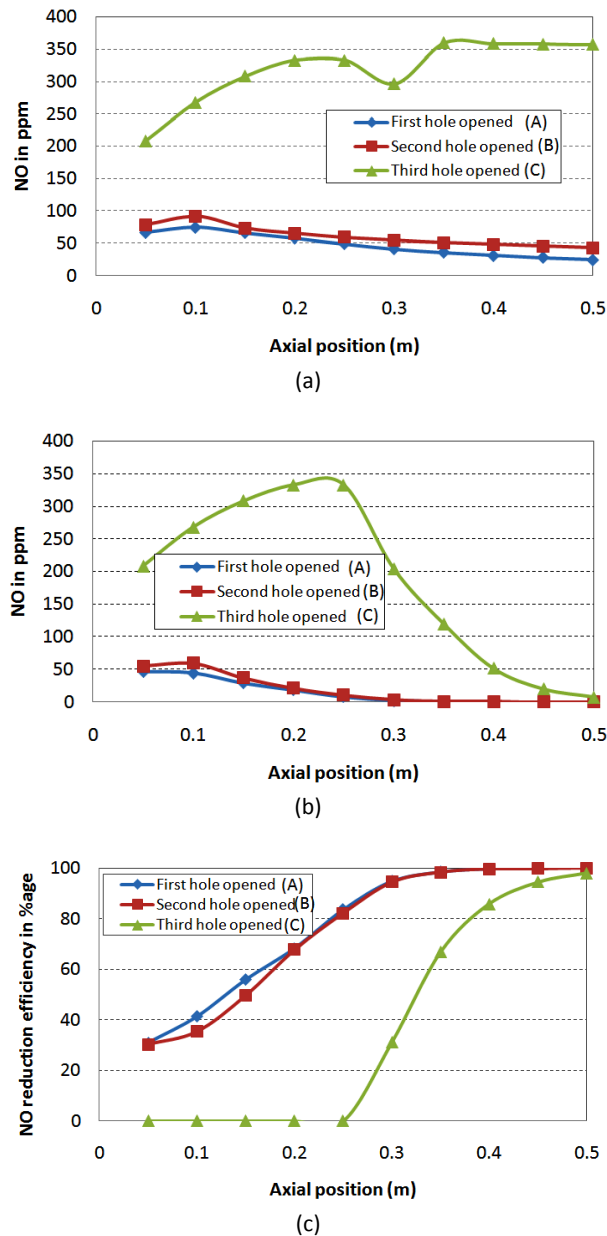


Fig. 12. (a) NO in ppm without reburn (b) NO in ppm with reburn and (c) NO reduction efficiency, for case A, B and C across different axial position

CONCLUSION

Computational simulation has been performed mainly to investigate the positional effect of reburn fuel injection on NO-reburn. The reburn fuel is injected radially at three different axial positions, whereas coal and air inject through a central hole. In case A, B and C, reburn fuel is injected at 0.1 m, 0.2 m and 0.3 m distance from inlet plane respectively. In this work coal-air mixture mass ratio is kept at a lower equivalence ratio, because with the addition of reburn

fuel, the overall equivalence ratio increases. The investigation is concluded with the following points.

(i) when the reburn fuel injection plane position is either at 0.1 m or 0.2 m from inlet plane, a high temperature flame has been observed near coal the inlet. Because in this region, a better combustible mixture is formed due to the reburn fuel pulling caused by the recirculation zone. On the other hand, when the reburn fuel is injected beyond the recirculation zone (0.3 m from the inlet plane), a low temperature flame exists at coal inlet region. Because in this region, the air-fuel mixture became lean due to the absence of reburn fuel. However a high temperature zone formed across reburn fuel injection plane due to presence of reburn fuel and with the presence of un-reacted air getting from lean mixture.

(ii) when the reburn fuel injection plane position is either at 0.1 m or 0.2 m from inlet plane, NO formation through all three sources has been observed in and around the flame that exists near coal inlet zone. High temperature flame in this region causes Thermal-NO formation. With the presence of reburn fuel in this region, sufficient hydrocarbon fuel produces hydrocarbon radicals. The subsequent reactions between hydrocarbon radicals with air nitrogen produce Prompt-NO. On the other hand, when injection plane is beyond the recirculation zone, a very small amount of Fuel-NO is formed in and around inlet flame region due to low flame temperature, but Prompt-NO and Thermal-NO exists only in and around downside flame due to higher downstream flame temperature and due to the presence of hydrocarbon radicals generated from reburn fuel respectively.

(iii) when the reburn fuel injection plane falls under the recirculation zone (fuel injection plane position at 0.1 m or 0.2 m from inlet plane), NO reduction efficiency increases along the length of the combustor and become maximum at the exit of the combustor (around 99.8%). In these cases NO reduction occurs much closer to coal inlet plane, due to presence of reburn fuel and higher flame temperature as well. On the other hand, when injection plane is located beyond the recirculation zone, NO reduction efficiency is 0% up to the length 0.25 m due to the absence of reburn fuel within this region. Beyond this position, the reduction efficiency increases and become highest at the exit of the combustor (around 98%). However it has been observed that reburn fuel injection plane placing closer to the coal inlet region has better NO reduction efficiency.

GRANT SUPPORT DETAILS

The present research did not receive any financial support.

CONFLICT OF INTEREST

The authors declare that there is not any conflict of interests regarding the publication of this manuscript. In addition, the ethical issues, including plagiarism, informed consent, misconduct, data fabrication and/ or falsification, double publication and/or submission, and redundancy has been completely observed by the authors.

LIFE SCIENCE REPORTING

No life science threat was practiced in this research.

NOMENCLATURE

A_p	Projected area of spherical particle		Greek Letters
c_{pg}	Specific heat	$d\Omega$	Solid angle
f_h	Fraction of energy transferred to gas phase formed due to volatile and char reaction	φ	Enthalpy in energy equation/ species mass fraction for various species in species transport equation
h_c	Heat transfer coefficient	ε	Dissipation of turbulent K.E.
I	Radiation intensity	γ	Stoichiometric air-fuel ratio
k	Generation of turbulent K.E./Kinetic rate	Γ	Diffusivity
MW	Molecular weight	θ	Radiation temperature
m	mass	σ	Prandtl number
m_{ash}	Mass fraction of ash obtained from proximate analysis	ρ	Density
m_{coal}	Mass flow rate of coal at inlet	$\bar{\tau}$	Stress tensor
$m_{coal\ outlet}$	Mass flow rate of coal at any cross-section	σ	Stefan Boltzmann constant
P_{FC}	Mass fraction of fixed carbon obtained from proximate analysis	ε_1	emmissivity
p	pressure	μ	Molecular viscosity
R	Universal gas constant		Subscript
S	Source terms	eff	effective
Sc	Schmidt number	lam	Laminar
T	Temperature	tur, t	Turbulent
t	time	g	gas
u	Velocity	s	solid
Y	Species mass fraction	m	mass
ΔH_v	Heat formation due to volatile reaction	p	particle
ΔH_c	Heat formation due to char reaction	vol	volatile
$-\bar{\rho} \overline{u_i'' u_j''}$	Reynolds stress tensor	i, j	Directional coordinates/ i^{th}, j^{th} particle, species.
		0	Initial state

REFERENCES

- Abbas, T., Costen, P., Hassan, M. A. and Lockwood, F. C. (1993). The Effect of the Near Burner Aerodynamics on Pollution, Stability and Combustion in a PF-Fired Furnace. *Combustion Science and Technology*, 93(1); 73–90.
- ANSYS FLUENT 14.0 Theory guide, 2011.
- Backreedy, R. I., Fletcher, L. M., Jones, J. M., Ma, L., Pourkashanian, M. and Williams, A. (2005). Co-firing pulverised coal and biomass: a modeling approach. *Proceedings of the Combustion Institute*, 30(2); 2955–2964.
- Backreedy, R.I., Fletcher, L.M., Ma, L., pourkashanian, A. and williams, A. (2006). modelling pulverised coal combustion using a detailed coal combustion model. *Combustion Science and Technology*, 178(4); 763–787.
- Bowman C.T., (1991). *Chemistry of gaseous pollutant formation and destruction*. U S Department of Energy, Office of Scientific and Technical information, New York. 250.
- Choi, C. R. and Kim, C. N. (2009). Numerical investigation on the flow, combustion and NOx emission characteristics in a 500MWe tangentially fired pulverized-coal boiler. *Fuel*, 88(9); 1720–1731.
- De S. and SOETE G. DE (1974). Overall reaction rates of NO and N₂ formation from fuel nitrogen.

- FIVELAND, W.A. (1988). Three-dimensional radiative heat-transfer solutions by the discrete-ordinates method. *Journal of Thermo physics and Heat Transfer*, 2(4); 309–316.
- Franchetti, B. M., Cavallo Marincola, F., Navarro-Martinez, S. and Kempf, A. M. (2013). “Large Eddy simulation of a pulverised coal jet flame. *Proceedings of the Combustion Institute*, 34(2); 2419–2426.
- Ghose, P., Patra, J., Datta, A. and Mukhopadhyay, A. (2016). Prediction of soot and thermal radiation in a model gas turbine combustor burning kerosene fuel spray at different swirl levels. *Combustion Theory and Modelling*, 20(3); 457–485.
- Gorenflo, R., Mainardi, F., Moretti, D., Pagnini, G. and Paradisi, P. (2002). Discrete random walk models for space–time fractional diffusion. *Chemical Physics*, 284(1-2); 521–541.
- Gu M, Zhang M, Fan W, Wang L, Tian F . (2005). The effect of the mixing characters of primary and secondary air on NO formation in a swirling pulverized coal flame. *Fuel*, 84(16); 2093–2101.
- Han, X., Wei, X., Schnell, U. and Hein, K. R. G. (2003). Detailed modelling of hybrid reburn /SNCR processes for NOX reduction in coal-fired furnaces. *Combustion and Flame*, 132(3); 374–386.
- Hashimoto, N., Kurose, R., Hwang, S.-M., Tsuji, H. and Shirai, H. (2012). A numerical simulation of pulverized coal combustion employing a tabulated-devolatilization-process model (TDP model). *Combustion and Flame*, 159(1); 353–366.
- HWANG, S.M., KUROSE, R., AKAMATSU, F., TSUJI, H., MAKINO, H. and KATSUKI, M. (2006). Observation of Detailed Structure of Turbulent Pulverized-Coal Flame by Optical Measurement. *JSME International Journal Series B*, 49(4); 1316–1327.
- LAUNDER, B. E. and SPALDING, D. B. (1983). The numerical computation of turbulent flows. *Turbulence and Combustion*, 96–116.
- Leung, K. M. and Lindstedt, R. P. (1995). Detailed kinetic modelling of C1 — C3 alkane diffusion flames. *Combustion and Flame*, 102(1-2); 129–160.
- Magnussen, B. F., & Hjertager, B. H. (1977). On mathematical modelling of turbulent combustion with special emphasis on soot formation and combustion. *Symposium (International) on Combustion*, 16(1); 719–729.
- Morsi, S. A. and Alexander, A. J. (1972). An investigation of particle trajectories in two-phase flow systems. *Journal of Fluid Mechanics*, 55(02); 193-208.
- Muto, M., Watanabe, H., Kurose, R., Komori, S., Balusamy, S. and Hochgreb, S. (2015). Large-eddy simulation of pulverized coal jet flame – Effect of oxygen concentration on NOx formation. *Fuel*, 142, 152–163.
- Ranz, W.E. and Marshall, W.R.(1952). Evaporation from drops. *Chemical Engineering progress*, 48(3);141-146.
- Saffari Pour, M., & Weihong, Y. (2014). Performance of pulverized coal combustion under high temperature air diluted by steam. *International Scholarly Research Notices*, 2014.
- Sahu, A.K. and Ghose, P. (2020). Computational modelling on pulverized coal combustion in a 5 kW burner to study NO reduction through Co-flow methane used as secondary fuel. *Computational Thermal Sciences, An International Journal*. 12(6); 555–578.
- Su, S., Xiang, J., Sun, L., Zhang, Z., Sun, X. and Zheng, C. (2007). Numerical simulation of nitric oxide destruction by gaseous fuel reburning in a single-burner furnace. *Proceedings of the Combustion Institute*, 31(2); 2795–2803.
- Su, S., Xiang, J., Sun, X., Zhang, Z., Zheng, C. and Xu, M. (2006). Mathematical Modeling of Nitric Oxide Destruction by Reburning. *Energy & Fuels*, 20(4); 1434–1443.
- Wen, X., Jin, H., Stein, O. T., Fan, J. and Luo, K. (2015). Large Eddy Simulation of piloted pulverized coal combustion using the velocity-scalar joint filtered density function model. *Fuel*, 158, 494–502.
- Wu, K.-T., Lee, H. T., Juch, C. I., Wan, H. P., Shim, H. S., Adams, B. R. and Chen, S. L. (2004). Study of syngas co-firing and reburning in a coal fired boiler. *Fuel*, 83(14-15); 1991–2000.
- YU, M. J., BAEK, S. W. and KANG, S. J. (2001). Modelling of Pulverized Coal Combustion with Non-Gray Gas Radiation Effects. *Combustion Science and Technology*, 166(1); 151–174.

- Zarnitz, R., & Pisupati, S. V. (2007). Evaluation of the use of coal volatiles as reburning fuel for NO_x reduction. *Fuel*, 86(4); 554–559.
- Zhang, X., Zhou, J., Sun, S., Sun, R., & Qin, M. (2015). Numerical investigation of low NO_x combustion strategies in tangentially-fired coal boilers. *Fuel*, 142; 215–221.

